

Investigating anode off-gas under spark-ignition combustion for SOFC-ICE hybrid systems

International J of Engine Research

1–16

© IMechE 2021

Article reuse guidelines:

sagepub.com/journals-permissions

DOI: 10.1177/14680874211016987

journals.sagepub.com/home/ijer



Zhongnan Ran¹, Jon Longtin and Dimitris Assanis¹

Abstract

Solid oxide fuel cell – internal combustion engine (SOFC-ICE) hybrid systems are an attractive solution for electricity generation. The system can achieve up to 70% theoretical electric power conversion efficiency through energy cascading enabled by utilizing the anode off-gas from the SOFC as the fuel source for the ICE. Experimental investigations were conducted with a single cylinder Cooperative Fuel Research (CFR) engine by altering fuel-air equivalence ratio (ϕ), and compression ratio (CR) to study the engine load, combustion characteristics, and emissions levels of dry SOFC anode off-gas consisting of 33.9% H₂, 15.6% CO, and 50.5% CO₂. The combustion efficiency of the anode off-gas was directly evaluated by measuring the engine-out CO emissions. The highest net-indicated fuel conversion efficiency of 31.3% occurred at $\phi = 0.90$ and CR = 13:1. These results demonstrate that the anode off-gas can be successfully oxidized using a spark ignition combustion mode. The fuel conversion efficiency of the anode tail gas is expected to further increase in a more modern engine architecture that can achieve increased burn rates in comparison to the CFR engine. NO_x emissions from the combustion of anode off-gas were minimal as the cylinder peak temperatures never exceeded 1800 K. This experimental study ultimately demonstrates the viability of an ICE to operate using an anode off-gas, thus creating a complementary role for an ICE to be paired with a SOFC in a hybrid power generation plant.

Keywords

Anode off-gas, syngas, spark ignition combustion, solid oxide fuel cell–internal combustion engine, variable compression ratio engine testing, zero dimensional modeling, hybrid power generation

Date received: 7 January 2021; accepted: 22 April 2021

Introduction

Over the past decades, global energy demand has increased significantly, leading to accelerated depletion of energy resources from fossil fuels and an increase in the production of air pollution and greenhouse gases. Among various environmentally sustainable solutions for the production of electrical energy, solid oxide fuel cells (SOFCs) can generate electricity with a high conversion efficiency while emitting relatively low emissions of pollutants. This is attributed to the inherent theoretical conversion efficiency advantage of SOFCs since electricity is generated directly from oxidizing the fuel instead of converting it to electricity by means of combustion.^{1–4}

A promising approach to increase electrical conversion efficiency and reduce emissions is the integration of SOFCs with downstream energy conversion devices such as gas turbines (GTs) and internal combustion

engines (ICEs).^{5–7} In a solid oxide fuel cell – gas turbine (SOFC-GT) energy system, the combustor is used to burn the high-exergy anode off-gas from the SOFC to produce extra shaft work for the hybrid system that is converted to electrical power. Hybrid SOFC-GT systems, although offering promising efficiency advantages, are limited to medium and large scale electricity generation applications because of the complexity, size, expense, and restrictive functioning characteristics of GTs. Interestingly, the general power generation capacity for GTs is typically in the megawatt (MW) range, which is an order of magnitude greater than SOFCs

Stony Brook University, Stony Brook, NY, USA

Corresponding author:

Dimitris Assanis, Stony Brook University, 100 Nicolls Road, Stony Brook, NY 11794, USA.

Email: dimitris.assanis@stonybrook.edu

generation capacity, typically in the kilowatt (kW) range.^{8–13}

Light-duty ICEs have a typical power generation capacity in the 100–200 kW range and can be used for distributed power generation and portable auxiliary field power unit applications.¹⁴ Additionally, an ICE can hybridize a SOFC power generation plant to further improve its overall electrical conversion efficiency and economic feasibility. Although the power density is lower for ICEs compared to GTs at high power generation ranges, it has been shown that ICEs can achieve higher thermal efficiency, while being more cost-effective than GTs operating at lower power generation ranges.¹⁵ Consequently, a system combining SOFCs with ICEs could derive additional benefits over the aforementioned hybrid SOFC-GT systems, including but not limited to, easier control of transient operating conditions, better fuel, and load versatility, as well as decreased manufacturing costs in low power generation requirement applications.

Several studies have explored the potential of SOFC-ICE systems. Lee et al.¹⁶ using the exergetic and exergoeconomic analysis method, showed that a SOFC-ICE hybrid system can achieve over 6% higher electrical efficiencies compared to a simple SOFC system. Based on modeling and exergy analysis of different configurations, Fyffe et al.¹⁷ concluded that coupling SOFC with an ICE was capable of achieving 70% electrical energy conversion efficiency for medium size hybrid systems. Colón Rodríguez et al.¹⁸ studied a SOFC-ICE system using a 100 kW engine and reported a 62% efficiency at a reformer temperature of 800 K with a 90% of fuel utilization in the fuel cell.

Choi et al.¹⁹ demonstrated that SOFC anode off-gas can be used as fuel in an ICE engine operating in homogeneous charge compression ignition (HCCI) mode, with a minimal amount of nitrogen oxide (NO_x) and total hydrocarbon (THC) emissions. Another SOFC-HCCI hybrid system for power generation was modeled by Zhu et al.²⁰ who predicted an energy conversion efficiency of 65.7%. Further, Park et al.²¹ modeled and compared SOFC-GT and SOFC-HCCI systems and reported that the latter could achieve an electrical efficiency of up to 60%, which is comparable to a SOFC-GT hybrid system. However, SOFC-HCCI hybrid systems have challenges associated with the added control complexity of HCCI combustion, which includes being highly sensitive to fuel chemistry, mixture composition, and thermal environment.²² Robust control strategies for HCCI combustion are needed to expand the operating range of the combustion mode and to handle the high heat release rates and pressure rise rates. The aforementioned HCCI combustion control challenges are further exaggerated during transient engine load operation due to the rapidly changing state conditions inside the combustion chamber.

An alternative advanced ICE concept that could potentially be paired with SOFCs includes jet-ignition combustion that utilizes one or multiple spark-ignited

pre-chambers to achieve lean burn combustion with a wider flexibility in required fuel chemistry, mixing composition, and thermal environment than HCCI.^{23,24} As pre-chamber engines are already used with gaseous fuels like compressed natural gas (CNG) for stationary power generation, this combustion mode is worth further exploring once ICEs are a proven match for SOFCs.

While advanced combustion modes and devices are being developed, the spark ignition (SI) ICE remains the most widely used device and combustion mode pairing. SI combustion provides simple and direct control over the start of ignition, and consequently combustion duration. It can also be readily coupled to a three-way catalyst, which is extremely efficient in reducing pollutant emissions under stoichiometric combustion. For the above reasons, the spark-ignition engine may be more suitable for the SOFC-ICE system than HCCI and SI pre-chamber engines presently. However, few computational or experimental studies have been conducted to quantify and analyze the performance, energy conversion efficiency, and emissions of a SI ICE operating on a realistic anode tail-gas composition from a SOFC. A multi-national renewable energy conglomerate developed a SOFC-SI engine system for burning anode off-gas, but experimental results have not been publicly reported.²⁵ More recently, Kim et al.²⁶ explored utilizing anode off-gas from a SOFC stack in an SI engine and reported a 61.6% system efficiency with significantly reduced levels of emissions of NO_x . Also, Ran et al.²⁷ experimentally studied and compared the simulated dry anode off-gas and traditional CNG with SI combustion conditions. It was found that engine-out emissions of NO_x were largely reduced, and THC was not present for the anode off-gas, but engine load was reduced in comparison to CNG fuel.

The work presented here builds upon the findings of Ran et al.²⁷ to address gaps in the literature, including the lack of detailed experimental and 0-D chemical kinetic modeling studies of the effects of SOFC anode off-gas compositions, specifically moisture content, on SI engine combustion, performance, and exhaust emissions. Therefore, the objective of this study is to experimentally explore the feasibility of a realistic SOFC anode off-gas as a potential alternative fuel under SI combustion conditions over a range of compression ratios (CRs), as well as to determine the fuel's compositional effects on engine thermodynamics, combustion characteristics, and emissions levels.

Hybrid SOFC-ICE plant

Hybrid system overview

In an effort to improve the electricity conversion efficiency of a SOFC generation plant, an ICE was added downstream of the fuel cell stack and used the anode off-gas as a fuel source in combination with ambient

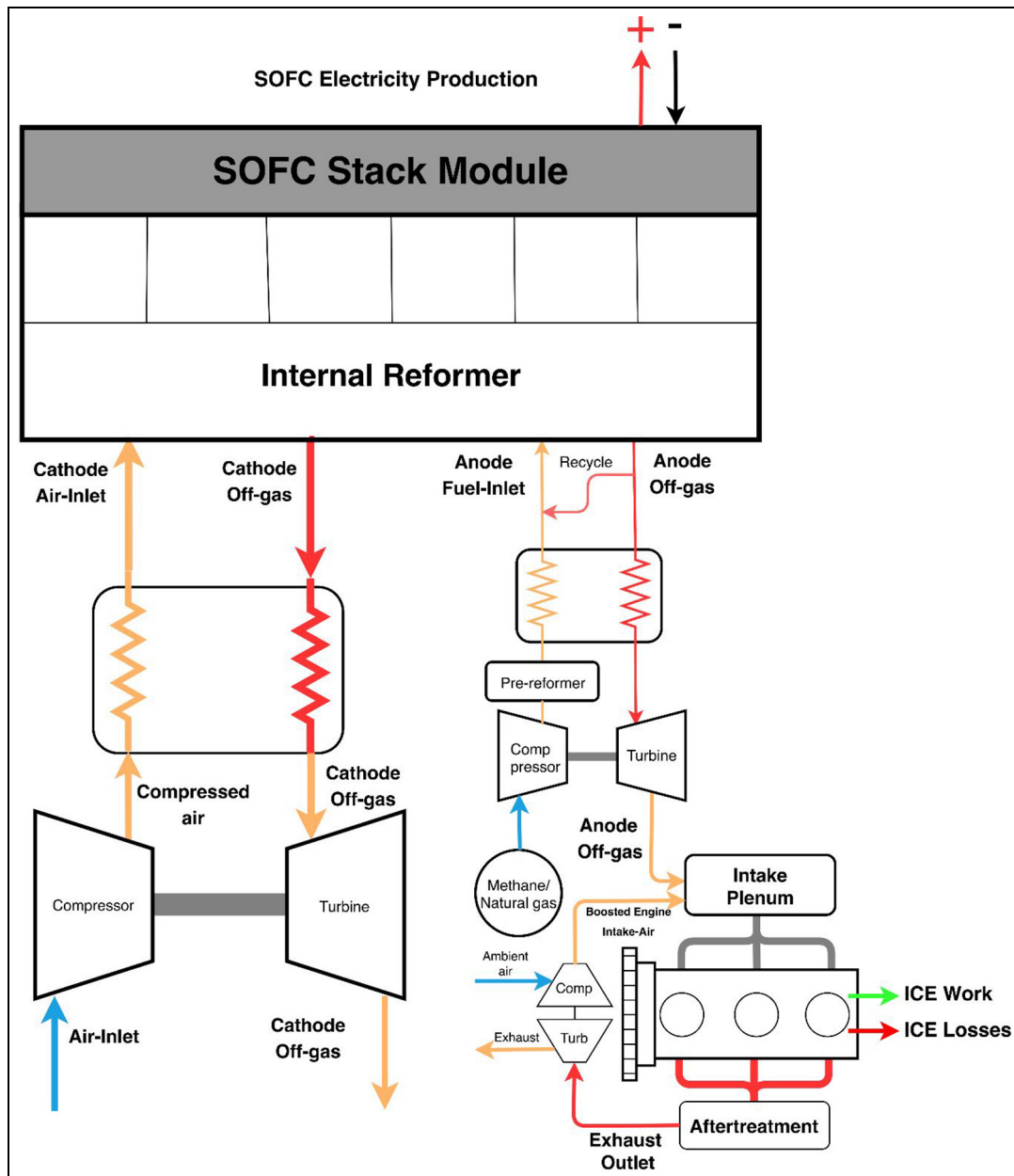


Figure 1. Detailed schematic for a representative SOFC-ICE hybrid system.

air as the oxidizer. A specific schematic of a representative SOFC-ICE hybrid power plant that has the theoretical potential to achieve 70% of system efficiency is shown in Figure 1. This representative hybrid system consists of two main devices that are the pressurized, high-temperature SOFC, and the ICE. Additionally, different types of reformers, compressors, expansion turbines, heat exchangers, and piping are needed to complete the remainder of the system.

To fuel the SOFC stack, methane (CH_4) is passed through an external, upstream, pre-reformer to form hydrogen (H_2), and carbon monoxide (CO). This primary fuel is then compressed to higher pressures and passed through a counter-flow heat exchanger before being fed into the internal reformer at an elevated pressure to form the syngas that is then fed into the SOFC

anode. Simultaneously, ambient air is compressed and passed through a counter-flow heat exchanger before being fed into the SOFC cathode. The syngas is electrochemically oxidized by the oxygen (O_2) contained in the compressed air to generate a potential difference between the anode and the cathode.

The high-temperature deoxygenated air from the cathode flows through a heat exchanger to preheat the incoming air before being expanded through a turbine. This produces shaft work that drives the compressor for the ambient air. In a similar fashion, the anode off-gas flows through the hot side of the heat exchanger in the anode system. After leaving the heat exchanger, the anode off-gas is expanded through a turbine that in turn drives the compressor that compresses the fresh CH_4 . The anode off-gas, composed of H_2 , CO , carbon

dioxide (CO_2), water (H_2O), finally exits the anode system. This off-gas can now be fumigated into the intake manifold, acting as the fuel source for a spark-ignited engine. The anode off-gas is mixed with fresh air in the intake manifold of the engine to form a homogeneous mixture for SI combustion. The shaft work provided by the reciprocating engine using the off-gas generates additional power for the hybrid system, thus improving its electrical energy conversion efficiency.

Anode off-gas composition

A previous study by Ran et al.²⁸ reported that syngas can be treated as a promising fuel for SI engines for improved engine efficiency and simultaneously leading to largely reduced THC and CO emissions compared to traditional fossil fuels. However, due to the high levels of diluent gases, the lower heating value of the anode off-gas is considerably lower compared to syngas, thus resulting in reduced laminar flame speeds. To improve the energy density and the ignitability of the mixture, most of the water vapor content must first be removed from the anode off-gas. This will result in the greatest chances to achieve robust combustion in a SI engine. Thus, it was of interest in these investigations to study both dry (containing 0% water vapor content) and simulated wet (containing up to 15% water vapor) anode off-gas compositions. This allowed for the composition effects of anode off-gas to be evaluated in terms of engine performance, combustion characteristics, and emission levels under SI combustion operation.

A representative SOFC with a gross efficiency of 65%, with 68% of molar fuel utilization and 51.1% recycling at the anode was selected to determine the actual anode off-gas composition needed for the experiments. Subsequently, an anode off-gas composition of 17.1% H_2 , 7.9% CO, 25.4% CO_2 , and 49.6% H_2O was used as summarized in Table 1. This composition comprises almost 25% volume of syngas (H_2 and CO) and is heavily diluted by water vapor (H_2O) and CO_2 as a result of the electrochemical process. Based on the above, a representative, as summarized in Table 1, dehydrated anode off-gas consisting of 33.9% H_2 , 15.6% CO, and 50.5% CO_2 was selected as the surrogate fuel.

Experimental facility and methodology

Experimental engine facility

All experiments were conducted at the Stony Brook University Advanced Combustion Laboratory

Table 1. Measured anode off-gas composition for the actual anode off-gas and surrogate fuel.

Fuel formation	H_2	CO	CO_2	H_2O
Actual (%)	17.1	7.9	25.4	49.6
Surrogate (%)	33.9	15.6	50.5	0

(SBU-ACL) located in the Advanced Energy Research and Technology Center. A single-cylinder Cooperative Fuel Research (CFR) engine with SI combustion mode was used for the experimental investigation of the surrogate anode off-gas. The overhead, two-valve cylinder head featured a combustion chamber with a spark plug mounted on the side. The CFR engine was a variable geometry engine that was capable of achieving a variable CR. Engine relevant details and geometric dimensions are presented in Table 2. Figure 2 provides a detailed diagram of the test engine setup.

An Alicat flow controller (MCRW-500SLPM-D/5M) placed before the intake was used to measure the intake air flow rate. A liquid fuel injection system allowed for the injection of liquid fuel into the intake port or the intake plenum. The mass flow rates of the injected liquids were metered with an Emerson Micromotion (CMFS0070) flow meter. The port fuel injection (PFI) system was converted to inject distilled water using the intake plenum fuel injector. The ignitable fuel source, the anode off-gas, was managed and metered with an additional Alicat mass flow controller (MCR-200SLPM-D/5M) before being delivered to the intake plenum to homogeneously blend with the inducted intake air during the intake stroke.

Engine brake torque and speed were measured through the DyneSystems InterLoc V controlled DC dynamometer. A piezoelectric pressure sensor (Kistler 7061B) mounted on the engine cylinder head was used for measuring the engine cylinder pressure. A Kistler 2629DK TDC sensor was used for high accuracy and dynamic determination of the CFR engine Top Dead Center (TDC) position. A BEI Precision optical crank angle encoder with a resolution of 0.2 crank angle degrees (CAD) was connected to the engine shaft for synchronization of shaft position. A Performance Electronics engine control management unit was utilized for the control over the spark timing and fuel injection timing during combustion.

An in-house data acquisition (DAQ) system built on a National Instruments (NI) cDAQ chassis was used to monitor low-speed and high-speed signals during experimentation. Measurement ranges and accuracy uncertainties for the recorded sensor signals are further detailed in Table 3. A LabVIEW VI was used for the collection of 200 engine cycles, and averaged values were post-processed with a MATLAB-based heat release analysis code.

Engine exhaust emissions were sampled using a heated line and measured with a Horiba MEXA-7100DEGR analyzer. The Horiba gas analyzer was calibrated for measurement of each species, listed in Table 4, at the beginning of each set of experiments using span gases corresponding with the respective concentration and species equal to the upper range of each measurement. The air-fuel ratio was measured using a ECM LambdaCAN pressure-compensated module outfitted with a NTK UEGO 6mA O_2 sensor. Emissions

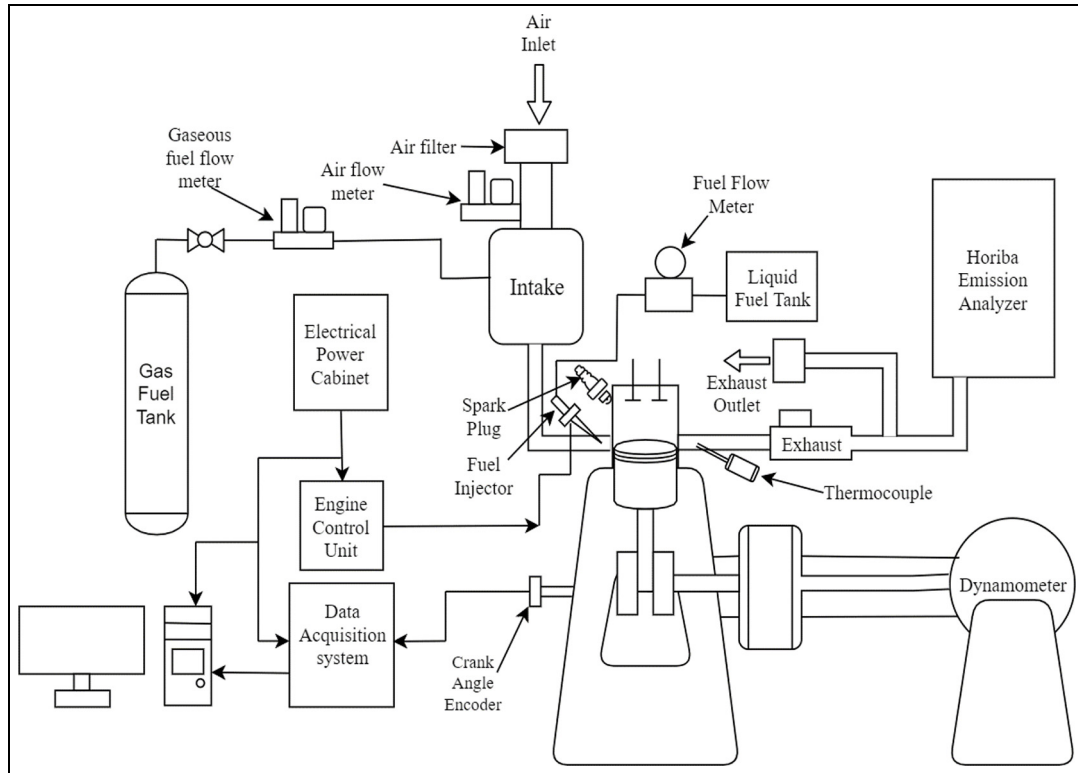


Figure 2. Detailed schematic of the CFR internal combustion engine facility.

Table 2. CFR engine detailed specifications.

Specification	Quantity
Engine cylinders	1
Engine valves	2
Stroke	114.3 mm
Bore	82.6 mm
Displaced volume	611.7 cm ³
IVO	−350° aTDC
IVC	−146° aTDC
EVO	140° aTDC
EVC	−345° aTDC
CR	6–18
Engine speed	1200 rev/min

measurement ranges and uncertainties are detailed in Table 4.

Experimental methodology

Experimental investigations of the anode off-gas with the CFR engine were conducted at a fixed engine speed of 1200 RPM with an intake manifold pressure of 75 kPa, since the engine operates optimally at this operating condition, to ensure high performance and thermal efficiency. The engine CR was individually fixed at 9:1, 11:1, and 13:1 to investigate its effects on engine performance, combustion processes, and levels of

Table 3. Instrument measurement ranges and accuracies in the CFR experimental facility.

Instrument	Range	Accuracy ^a
Pressure transducer	0–250 bar	≤ ±0.05% FS
Alicat mass flow controller MCRW-500SLPM-D/5M	0–500 SLPM	±0.8% RD + 0.2% FS
Alicat mass flow controller MCR-100SLPM-D/5M	0–100 SLPM	±0.8% RD + 0.2% FS
Micromotion flow meter CMFS007	0–40.9 kg/h	±0.1% liquid Mass/volume flow rate
Crank encoder	0–30,000 RPM	±0.5 bit
Dynamometer	0–4500 RPM	N/A
Thermocouples (type K)	−200°C to 1250°C	> 2.2°C or 0.75% RD
Lambda sensor	0.7–∞	±0.2 for λ = 1.70 ±0.04 for λ = 0.80

^aAbbreviation stand for the percentage of full scale (% FS) and percentage of reading (% RD).

Table 4. Emissions measurement ranges and accuracies at the CFR experimental facility.

Species	Range	Error ^a
CO (L)	0–5000 ppm	Linearity within $\pm 1.0\%$ FS or $\pm 2.0\%$ RD
CO (H)	0%–5%	
NO _x	0–3000 ppm	Repeatability within $\pm 0.5\%$ FS or $\pm 0.5\%$ RD
UHC	0–10,000 ppm	
O ₂	0%–18%	Drift within $\pm 1.0\%$ FS or $\pm 1.0\%$ RD
CH ₄	0–3000 ppm	
CO ₂	0%–15%	

^aAbbreviation stand for the percentage of full scale (% FS) and percentage of reading (% RD).

emissions. To achieve the desired anode off-gas compositions as stated previously, each of the individual constituents was supplied from Airgas company compressed gas bottles with a tolerance on targeted mixture composition of $\pm 2\%$.

The engine was motored, allowed ample time to achieve steady-state operating conditions, and baselined before conducting the experiments. During the studies, maximum brake torque (MBT) was selected by sweeping the spark timing. Ultimately, the engine spark timing was set such that the crank angle where 50% of heat is released, defined as *CA50*, was kept around 6° – 12° after top dead center (aTDC) to ensure optimal engine thermal efficiency. Fuel air-charge mixtures were varied during experimentation through a targeted equivalence ratio, ϕ , sweep ranging from stoichiometry, $\phi = 1.0$, down to $\phi = 0.60$, in 0.05 of targeted decrements. Note that the actual, experimentally determined equivalence ratios and not the targeted equivalence ratios were used during the creation of the comparative figures shown in the results and discussion.

To quantify the effect of water vapor on the combustion characteristics of the dry surrogate anode off-gas, liquid distilled water was injected into the intake plenum of the engine, far enough upstream of the intake valve, to ensure sufficient time for evaporation and mixing. Volume fractions of 5%, 10%, and 15% were injected at selected fuel-air equivalence ratios, that is, at stoichiometry and the lean equivalence ratio point.

Results and discussion

Engine volumetric efficiency, mass flow rate of air and fuel

Engine volumetric efficiency can be used to evaluate the breathing capacity of an engine during the intake stroke.²⁹ The following formula was used for the calculation of the volumetric efficiency: $\eta_v = \frac{\dot{m}_a \times n_r}{\rho_a \times V_d \times N_e}$, where \dot{m}_a is the mass flow rate of air, n_r is the number of crankshaft rotations for a complete engine cycle (2 for 4-stroke), ρ_a is the intake air density, V_d is the engine displacement, and finally N_e is the engine speed. The intake process for the anode off-gas operated in

the CFR engine is presented in Figure 3, quantifying (1) the volumetric efficiency, (2) the mass flow rate of air, and (3) the fuel flow rate associated with the ϕ , for CR of 9:1, 11:1, and 13:1. As shown in Figure 3, the volumetric efficiency when using anode off-gas as fuel is considerably reduced compared to operation with conventional liquid or gaseous fuels, such as gasoline and CNG.²⁸ This is mainly due to the significantly smaller (1.25:1) stoichiometric air-fuel ratio of the anode off-gas, versus 14.7:1 with gasoline and 17.2:1 for CNG, therefore allowing a larger volume of gaseous fuel to enter the combustion chamber, which displaces intake air. Note that the low heating value of the off-gas anode fuel drives the need for this proportionately larger volume of gaseous fuel to match the energy content of conventional fuels.

Additionally, the fuel composition of anode off-gas has 50.5% of CO₂, thus the overall fuel energy density is significantly lowered when compared to conventional fossil fuels. Therefore, it is obvious that the fuel flow rate had to be largely increased to achieve the same energy content to match the engine load conditions. As a result, the air displacing effect was exaggerated as shown in the fuel flow rate plot.

The experimental results presented in Figure 3 show that the volumetric efficiency and the rate of fuel flow are both inversely proportional to increasing ϕ at both CRs evaluated. Increasing the charge mixture ϕ while maintaining a constant manifold pressure of 75 kPa requires simultaneously decreasing the mass flow rate of fuel injected while increasing the mass flow rate of ambient air flown into the intake system. Since the anode off-gas is fumigated into the intake plenum in gaseous form, increasing the fuel-air equivalence ratio requires increasing the mass of fuel injected, which results in displacing ambient air from the plenum and thus lowers the mass flow rate of the air, consequently, the volumetric efficiency.

The air flow rate and volumetric efficiency increase observed in Figure 3 from CR 9:1 to 13:1 are attributed to the decrease in the combustion chamber clearance volume, thus decreasing the residual gas fraction and in turn improving the volumetric efficiency. On the other hand, the fuel flow rate decreased from CR 9:1 to CR

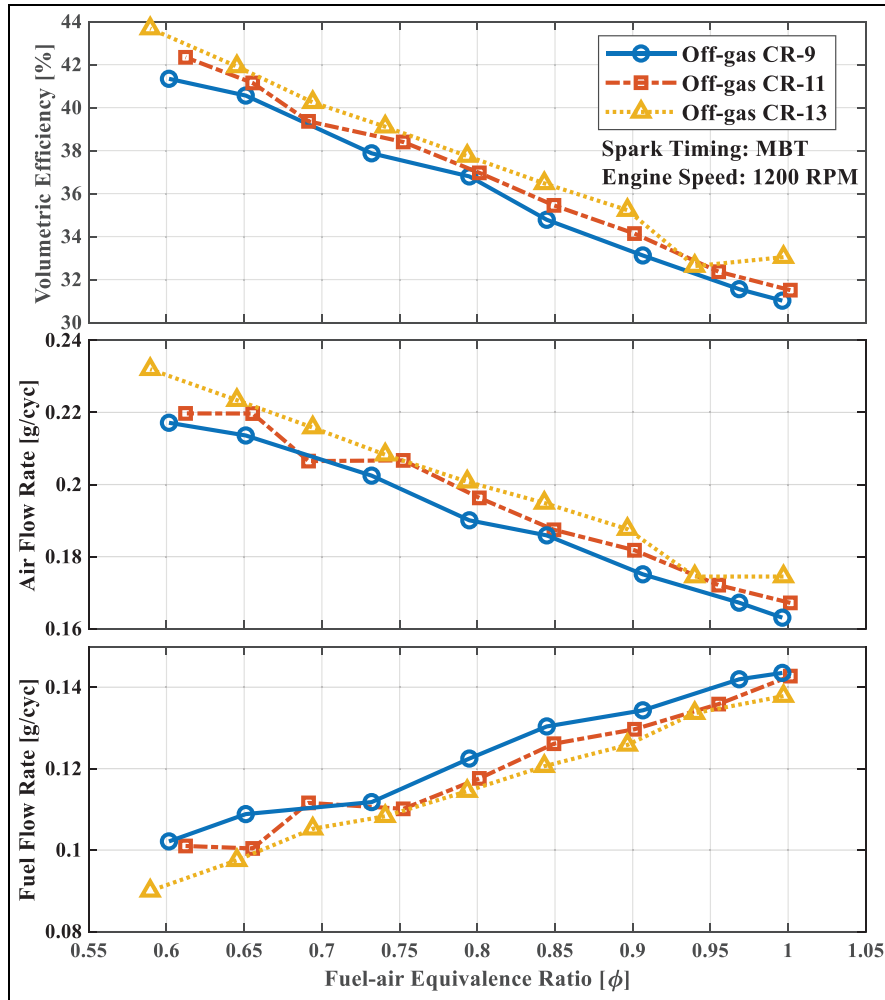


Figure 3. Volumetric efficiency, air, and fuel flow rate for anode off-gas as a function of ϕ .

13:1 is due to more fuel displaced by the air when the air flow rate is increased.

Net indicated mean effective pressure

The net indicated mean effective pressure ($IMEP_{net}$) measures the ability of an engine to generate work, independent of engine displacement. This parameter is determined by integrating the pressure trace over the entire thermodynamic cycle, allowing the engine performance to be directly evaluated without having to measure the frictional losses.

The experimental results were analyzed to determine the $IMEP_{net}$, shown in Figure 4, with respect to ϕ at CR of 9:1, 11:1, and 13:1. The $IMEP_{net}$ is determined to proportionally increase with ϕ for every engine CR investigated. This trend is anticipated as the leaner air-fuel mixtures hold a smaller amount of fuel to reach the targeted ϕ , thus causing the input energy content per cycle to decrease. Further enleanment of the charge mixture yields decreasing flame propagation speeds and consequently decreases combustion rates, which clarifies the resulting relationship between $IMEP_{net}$ and ϕ . This trend aligns with the typical combustion

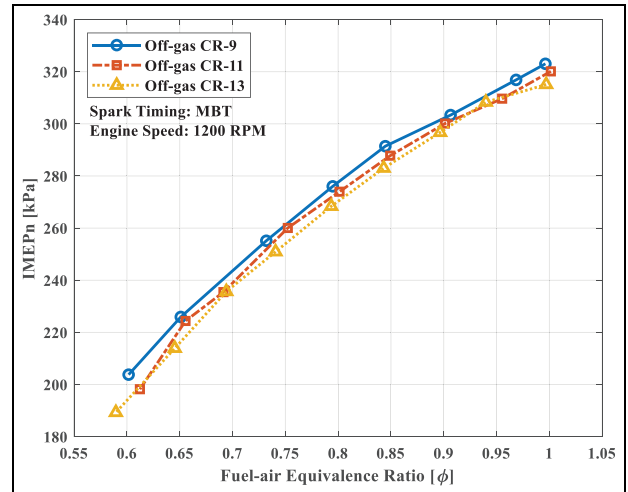


Figure 4. Engine $IMEP_{net}$ for anode off-gas as a function of ϕ .

characteristics of conventional fuels, such as gasoline and CNG, in a SI ICE. Due to experimental error, there exists a slight variation in the actual ϕ reported between the three CR data sets, although the same charge-mixture conditions were targeted. This small

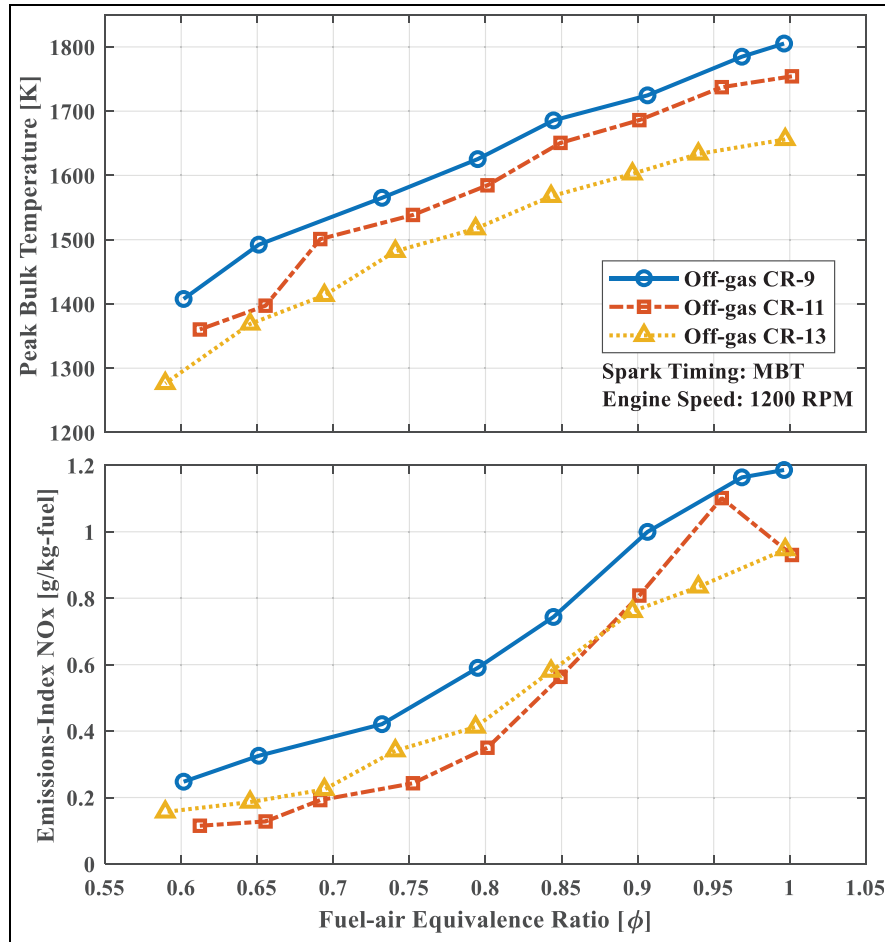


Figure 5. Peak temperature and emissions index of NO_x for anode off-gas as a function of ϕ .

Table 5. Mean and standard deviation of COV_{IMEP}

CR	Mean (%)	Standard deviation (%)
9:1	0.67	±0.13
11:1	0.68	±0.29
13:1	0.83	±0.28

deviation in ϕ was within expected experimental testing variation; it is an artifact of trying to delicately balance changing boundary conditions while dealing with a total run-time-constraint limited by the amount of anode off-gas mixture in each compressed cylinder. With that stated, it was deemed more important to ensure the engine cyclic variability was minimized ($< \pm 5\%$) during combustion and data collection than trying to decrease the experimental targeted conditions in ϕ . The coefficient of variation in indicated mean effective pressure (COV_{IMEP}) can be used to define the cyclic variability in indicated work per cycle. Table 5 shows the average and standard deviation of COV_{IMEP} at CRs of 9:1, 11:1, and 13:1 within the experimental ϕ range tested. The averages of the COV_{IMEP} are all well below the desired 5% threshold, indicating steady-state combustion operation is achieved.²⁹

The increase in the engine CR from 9:1 to 13:1, however, did not result in an improvement in the engine output performance, as expected. This is because the MBT spark timing needed to be adjusted to maintain combustion phasing increasing CR. Ultimately, the three CRs studied yield somewhat similar engine output performance for the anode off-gas. Further, the IMEP_{net} results, shown in Figure 4, demonstrate the feasibility of a hybrid system to generate additional power by burning anode off-gas, originating from a SOFC stack, downstream of an ICE.

Cylinder peak bulk temperature and emissions index of NO_x

The engine peak bulk temperature and NO_x emissions as a function of ϕ , at CRs of 9:1, 11:1, and 13:1 are presented in Figure 5. The peak bulk temperature was defined as the mass-averaged temperature over the engine combustion cycle and can be calculated based on the ideal gas law, once the total trapped mass, cylinder pressure, cylinder volume, and gas constant R are known.²⁹ The engine cylinder bulk temperature decreases proportionally with decreasing charge-mixture ϕ . This anticipated outcome is a result of leaner charge-mixtures

containing less energy content, which in turn results in slower flame propagation rates. The decreased propagation rates are translated to decreased heat release rates, which ultimately achieve a decreased overall cylinder temperature as the charge mixture becomes leaner. The engine cylinder bulk temperature was the lowest at the highest CR of 13:1, due to MBT spark timing retardation to avoid violent pressure rise rates. Retarding the MBT spark timing caused the combustion phasing to be retarded, thus phasing the combustion later in the expansion stroke, reducing the heat release rate, and ultimately lowering the cylinder bulk temperature. The decreased engine cylinder temperature negatively affected the engine combustion efficiency and CO emissions due to reduced oxidation rates. However, as shown in Figure 5, keeping the overall cylinder temperature below the 1800 K NO_x formation limit²⁹ resulted in negligible NO_x emissions ($< 1.2 \text{ g/kg-fuel}$). Even at such low NO_x values, as ϕ is leaned out from the stoichiometric operating condition, the NO_x emissions are further decreased to nearly zero as we approach the lean misfire limit of $\phi = 0.60$. Specifically, an increase in CR from 9:1 to 11:1 resulted in lower NO_x emissions, and increasing the CR from 11:1 to 13:1, slightly decreased NO_x emissions from stoichiometry until $\phi = 0.90$, and slightly increased NO_x emissions for charge-mixtures leaner than $\phi = 0.90$. It is also worth noting, the range of NO_x emissions measured fall near or below the minimum detection threshold of the emissions analyzer utilized in these experiments. Thus, it can be concluded that combustion with anode off-gas in a SI engine resulted in minimal to undetectable NO_x emissions. This significantly low amount of engine-out NO_x emissions demonstrates that the anode off-gas is a viable fuel source that offers a cleaner combustion process, as compared to conventional fossil fuels such as gasoline and CNG.

Engine combustion efficiency and emissions index of CO

Given that the combustible reactants in the anode off-gas are H_2 and CO, it is expected that the THC and soot emissions are negligible since the fuel contains no hydrocarbon species, and the air-fuel mixture was formed homogeneously before entering the combustion chamber. This was also verified in the experimental studies performed for this work as the THC and soot emissions measurements were minimal, with specific emissions levels of zero, and thus are not reported in greater detail. Further, it is assumed that the H_2 present in the charge-mixture is entirely consumed during combustion due to the high reactivity of this species coupled with an extremely low ignition energy requirement of 0.011–0.017 mJ for the H_2 -air mixture; this requirement is readily met, in contrast to more conventional hydrocarbon fuels. On the other hand, the CO-air mixture during combustion requires a substantially higher ignition energy than the H_2 -air mixture.^{30,31}

Thus, there is a critical need to track and report the engine-out CO to assess the combustion efficiency when using anode off-gas during combustion.

Combustion efficiency can be used to evaluate the completeness of the combustion process when reactants are transformed into products, and it was calculated using the following formula: $\eta_c = \frac{\dot{m}_{\text{CO},i}}{\dot{m}_{\text{CO},e}}$, where $\dot{m}_{\text{CO},i}$ is the mass flow rate of CO into the engine, and $\dot{m}_{\text{CO},e}$ is the mass flow rate of CO exit of the engine after combustion. It was expected that the anode off-gas charge mixture would have a strong inverse correlation to the amount of engine-out CO, as this will be a direct indicator that the lesser-reactive species was not consumed during combustion. For traditional fossil fuels used during combustion, the engine combustion efficiency is determined using the exhaust emissions of CO_2 , CO, and THC. However, the determination of combustion efficiency when using anode off-gas as fuel is more accurate by using only the CO content found in the exhaust gas that has not been transformed into CO_2 . The emissions of THC is expected to be minimal in the combustion of this surrogate fuel. The engine combustion efficiency as a function of ϕ , at CRs of 9:1, 11:1, and 13:1 is presented in Figure 6. Experimental data showed that combustion efficiency is inversely proportional to engine-out CO. This is an expected outcome given that CO is one of the reactants in the anode off-gas combustion, thus higher oxidation of CO to CO_2 yields higher combustion efficiency. An increase in CR from 9:1 to 13:1 resulted in reduced combustion efficiency. This was an anticipated finding and related to the knock-limited experimental data at CR of 13:1, requiring MBT spark timing to be retarded, which in turn lowered the peak cylinder temperature. This negatively affected the oxidation of CO, and hence the combustion efficiency is lower at CR of 13:1 compared to CRs of 9:1 and 11:1.

The CO emissions index as a function of ϕ at CRs of 9:1, 11:1, and 13:1 is presented in Figure 6, as well. The CO emissions are largely reduced when the ϕ is leaned out from stoichiometric condition to $\phi = 0.95$. When ϕ is further decreased, an increase in CO emissions is observed. Reduction of CO emissions occurs when there is excess oxygen present during combustion, as ϕ is decreased below stoichiometric, which helps the formation of CO_2 from CO. In parallel, as ϕ is reduced, the energy content of the mixture is reduced, causing decreased overall combustion peak temperatures. Clearly, there exists a trade-off point between increased oxygen concentration in the cylinder and peak bulk temperatures remaining at adequately high values for converting CO to CO_2 . As a result, CO_2 emissions peak at $\phi = 0.95$ for SI combustion with anode off-gas.

It should be noted that a CR increase from 9:1 to 13:1 resulted in a significantly increased level of emissions of CO, due to the crevice storage effect for the particular design of the combustion chamber of the

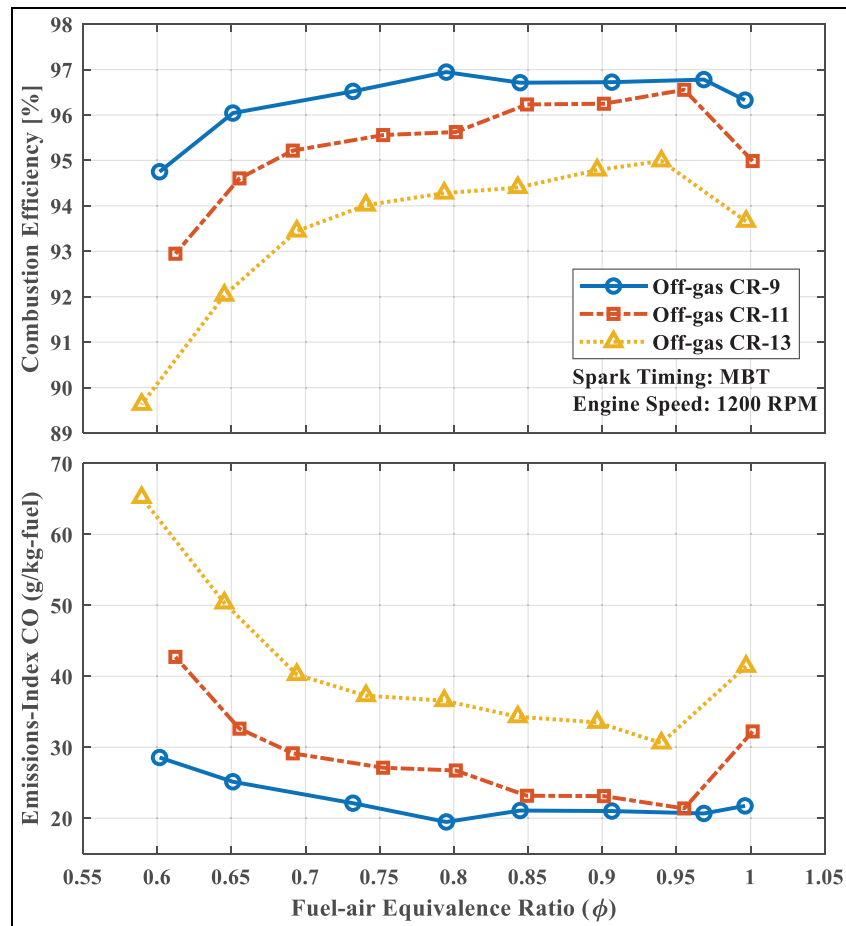


Figure 6. Combustion efficiency and emissions index of CO for anode off-gas as a function of ϕ .

CFR engine. At higher CRs, there is higher pressure before ignition, therefore, larger quantities of the air-fuel mixture are stored in the crevices. This required the spark timing to be retarded. This further reduced cylinder peak temperatures and resulted in higher CO emissions at the higher CR of 13:1, due to lower combustion temperature and higher unburned CO emissions from the crevices into the exhaust. Additionally, the increase in CO when CR is increased is also likely because of the flame quenching associated with the reduced squish heights.

Net-indicated fuel conversion efficiency and fuel consumption

The experimental results were analyzed to determine the engine indicated net fuel conversion efficiency and fuel consumption as a function of ϕ , as shown in Figure 7, at CRs of 9:1, 11:1, and 13:1. As presented in Figure 7, anode off-gas with SI combustion achieved a net indicated fuel conversion efficiency of 31.3% and fuel consumption of 2490 g/kWh at CR of 13:1. While these efficiency levels are potentially lower than the typically expected levels for a modern SI engine, the goal of this study is to demonstrate the feasibility of burning a realistic anode tail-gas composition in SI

combustion over a range of geometric CRs. These findings successfully proved the viability of utilizing the SOFC anode off-gas as a potential fuel in SI engines. It is important to note that this CFR engine is not designed to maximize efficiency, with the side-mounted spark plug, two valves per cylinder, and low levels of turbulence all contributing to longer burn durations and lower efficiencies than a modern SI engine. Hence, this reasoning allows us to conclude that the net indicated fuel conversion efficiency of the anode off-gas would be even greater than 31.3% if burned in a modern architecture SI engine that featured shorter burn duration times.

As presented in Figure 7, as ϕ was decreased from stoichiometry, the net indicated fuel conversion efficiency started to increase at first, before eventually decreasing. The trend for fuel consumption is exactly the opposite since the indicated fuel consumption has a strong inverse correlation to the fuel conversion efficiency. These trends are indicative of a trade-off that is maximized within the range of experimental data collected. As the charge-mixture ϕ becomes leaner, and thus more ambient air is present in the charge-mixture, the ratio of specific heats (γ) of the charge-mixture increases, which positively benefits net indicated fuel conversion efficiency and fuel consumption during

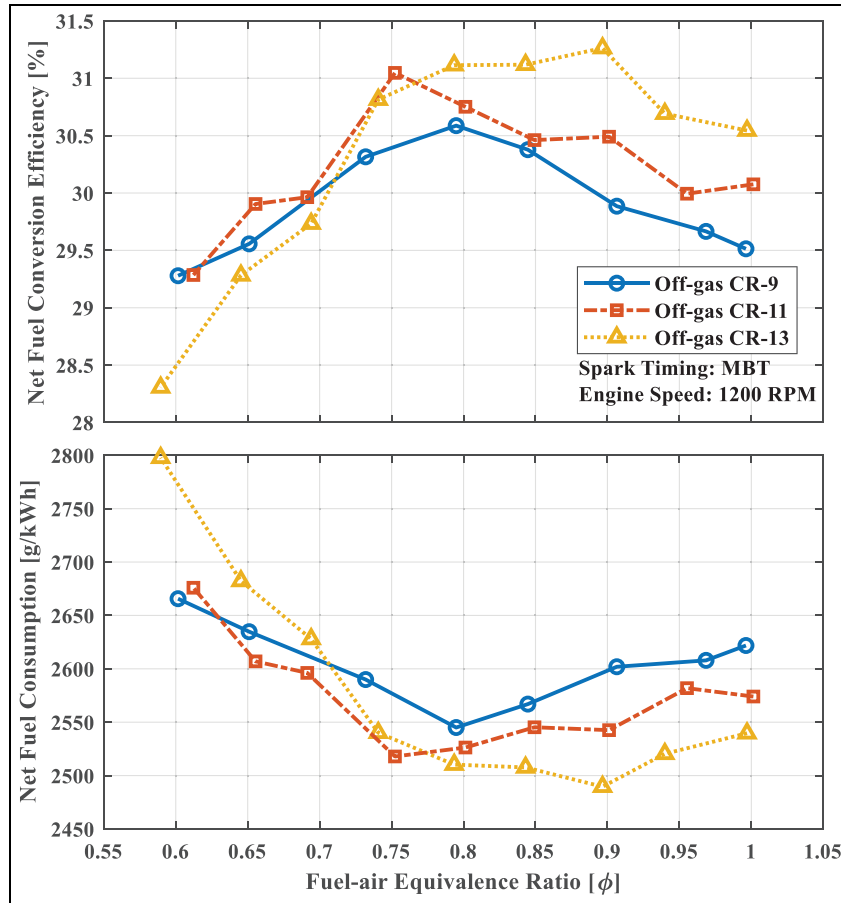


Figure 7. Fuel conversion efficiency and fuel consumption for anode off-gas as a function of ϕ .

combustion. Further, the reduction in engine bulk temperature, as the charge-mixture ϕ decreases, causes a decrease in the heat transfer rate; this positively benefits the fuel conversion efficiency and fuel consumption as well. Ultimately, as ϕ becomes leaner, the combustion becomes less robust as it approaches the lean limit. As the fuel conversion efficiency is decreased, consequently, the fuel consumption is increased due to the occurrence of misfiring, incomplete combustion, and the lengthened burn duration. Thus, the optimum trade-offs for the net indicated fuel conversion efficiency and fuel consumption of anode off-gas are achieved at $\phi = 0.80$, $\phi = 0.75$, and $\phi = 0.90$ for CR of 9:1, 11:1, and 13:1, respectively. Increasing CR to 13:1 helped increase the fuel conversion efficiency and decrease the fuel consumption. This is attributed to the higher associated expansion ratio and lower heat transfer rates; those are driven by the decreased overall cylinder temperature, caused by the knock-limited, retarded, MBT combustion phasing.

Engine combustion phasing and combustion duration

The crank angle position where 50% of the mass fraction is burned (CA50) can be used as a metric that indicates the combustion phasing. Meanwhile, the crank

angle interval between 10% and 90% of the mass fraction burned (CA10-90) is used to describe the overall combustion duration. In the SI engine, the start and duration of the combustion process itself are directly affected by the spark timing; and the amount of charge-mixture consumed is dependent on the heat release rate, which in turn is ultimately dominated by flame propagation rates and charge motion.

The experimental results were analyzed to determine CA50 and CA10-90 as a function of ϕ , as shown in Figure 8, at CRs of 9:1, 11:1, and 13:1. For CRs of 9:1 and 11:1, the CA50 was maintained at around 6° – 10° aTDC, to ensure optimal engine output performance and efficiency. For CR of 13:1, the CA50 is phased later than the other CRs. This is due to engine performance being knock-limited at higher CRs, especially at higher charge-mixture equivalence ratios, and thus requiring the spark-timing to be retarded to avoid knock. This changes the start of combustion, which affects the heat release profile of the charge-mixture, and consequently, it takes more crank angles to burn 50% of the charge-mixture. Similarly, as shown in the combustion duration, since the spark timing for CR of 13:1 was retarded, the lower in-cylinder pressure and heat release caused the CA10-90 to be longer than that of CRs of 9:1 and 11:1. As the ϕ is decreased toward

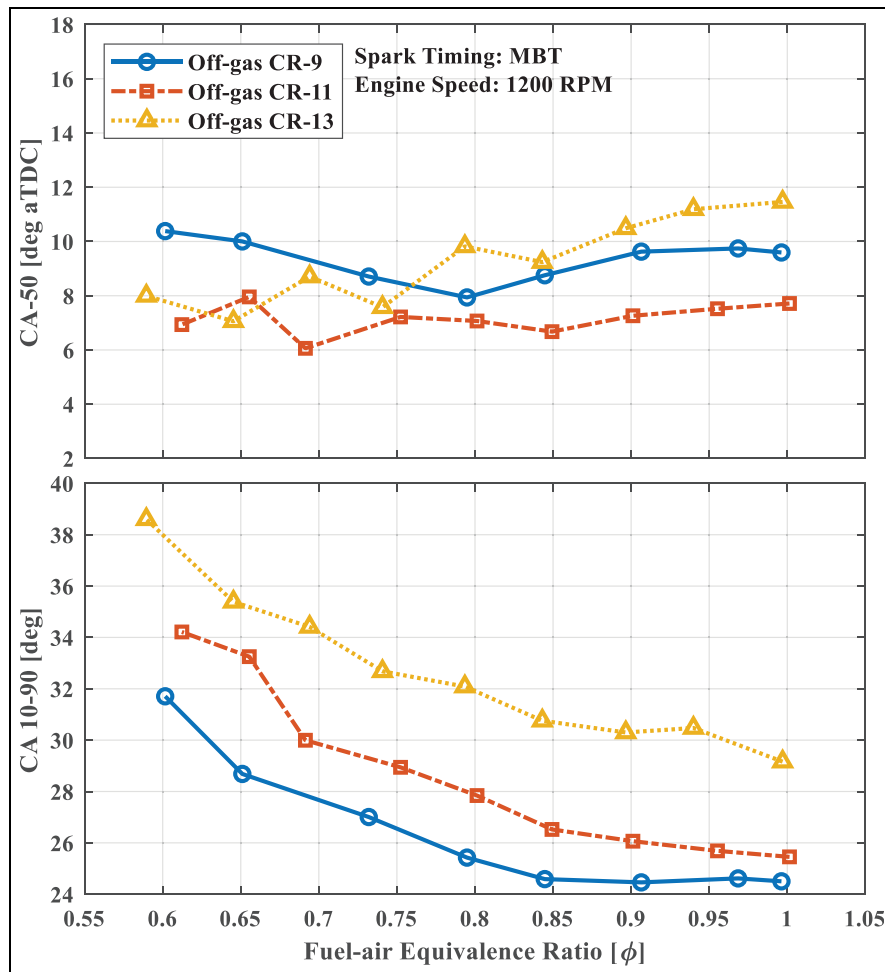


Figure 8. CA-50 and CA10-90 for anode off-gas as a function of ϕ .

leaner conditions, the overall energy density of the air-fuel mixture is reduced as well, consequently, the air-fuel mixture is less prone to engine knock. This permits the leaned-out mixtures at higher CRs to maintain comparable CA50 as mixtures ignited at lower CRs. However, the combustion duration (CA10-90) is increased due to the slower flame speed and reduced fuel oxidation rates caused by less energy input at lean conditions.

Compared to previous experimental studies presented by Choi et al.¹⁹ the use of SI instead of HCCI combustion mode has several advantages. The direct control of initiating combustion through a spark discharge allows for precise and predictable combustion phasing control. This allows the engine to be calibrated more robustly and achieve a wider operating range with higher efficiencies than what is commonly achieved through HCCI combustion mode.

Effect of water vapor on peak bulk temperature, cylinder pressure, and combustion rates

The composition of the surrogate SOFC anode off-gas as it exits the stack includes 49.6% of water vapor and is formed during the electrochemical process. The water

vapor reduces the energy content of the anode off-gas on a molar basis and thus increasing the mass flow rate of gas that flows through the engine downstream of the stack. Therefore, the experimental results presented so far have been collected using a dry anode off-gas from which the water vapor has been removed. Removing the water increases the volumetric energy density of the anode off-gas and increases the concentration of H_2 and CO in the mixture, making it more conducive to SI combustion. However, removing the entire amount of water vapor from the anode off-gas may not be easily achievable in a hybrid SOFC-ICE system. Therefore it is critical to investigate the effects of water vapor in the mixture, which acts as a diluent in addition to CO_2 .

In this study, water was injected into the intake plenum to investigate the effects of water content on combustion characteristics. However, due to the physical limitations on the injector opening duration, only concentrations up to 15% by volume of anode off-gas were injected. SI combustion with the simulated wet anode off-gas was analyzed at stoichiometry and $\phi = 0.75$. The effect of water vapor on cylinder peak temperature as a function of ϕ at a CR of 11:1 is shown in Figure 9. Figure 10 shows the gross heat release rate and cylinder

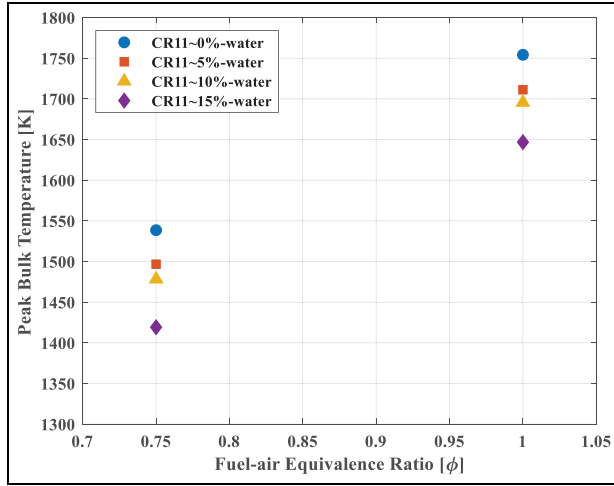


Figure 9. Peak bulk temperature of CR 11:1 as a function of ϕ and water vapor percentage.

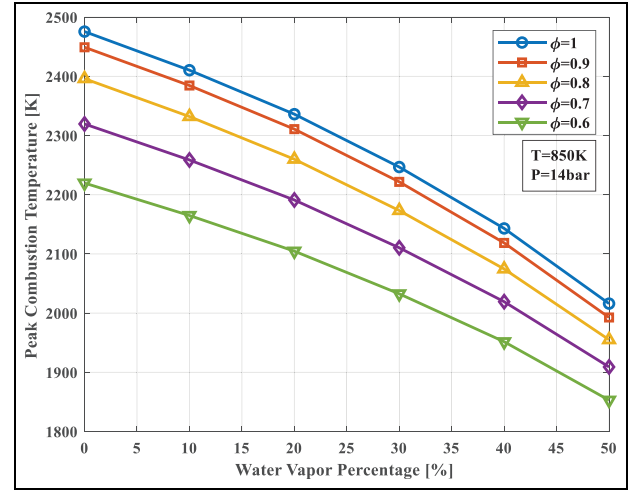


Figure 11. Peak combustion temperature as a function of ϕ and water vapor percentage.

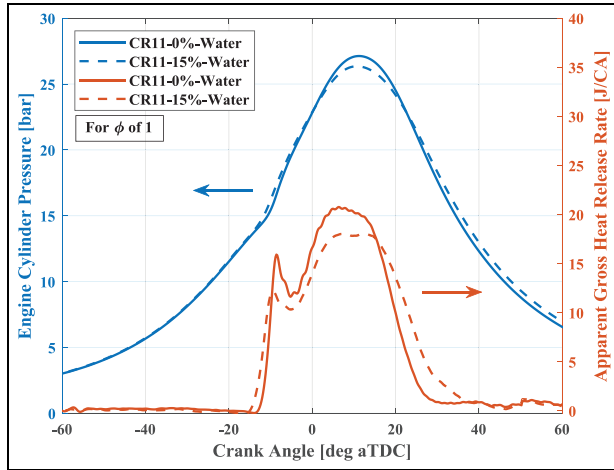


Figure 10. Cylinder pressure and combustion rates for stoichiometric operation at a CR of 11:1 with two levels of water vapor content in the anode off-gas, 0%, and 15%.

pressure for stoichiometric operation with dry and wet off-gas with 15% volume water vapor content.

Introducing water vapor into the anode off-gas mixture reduced its energy density and increased its heat capacity, c_p . The result was lower heat release compared to operation with dry off-gas, reduced cylinder pressure and temperature, reduced work production, and ultimately reduced fuel conversion efficiency. Based on this result, in a hybrid SOFC-ICE system, it is critical to limit the water vapor that enters the engine with the off-gas so that the volumetric efficiency, load, and fuel conversion efficiency are maximized. However, if the engine is required to operate with some water vapor content in the off-gas due to system constraints, then its performance can be improved through additional means, such as intake boosting, increased CR, or a combustion chamber design that accelerates flame propagation and increases the heat release rates.

0-D modeling of the effects of water content

The work presented above experimentally investigated the effects of adding water vapor on the combustion characteristics of anode off-gas in SI combustion mode. However, due to the physical limitation on the port fuel injector, only up to 15% of water vapor was injected during combustion. Also, water vapor was only injected at selected equivalence ratios. Based on the proposed SOFC-ICE hybrid system, the actual composition of the anode off-gas contains up to almost 50% of water vapor, which will significantly affect the physicochemical properties of the fuel. Therefore, to fully understand the impacts of adding 50% of water vapor on the fuel properties and combustion processes, a 0-D constant volume combustion model was developed in Chemkin-Pro. A homogeneous closed batch reactor was modeled to study the variations of peak combustion temperature, laminar flame speed, as well as ignition delay times under constant volume conditions. The chemical mechanism developed by NUI-Galway³² containing 15 species and 48 reactions was used to model syngas with H_2 and CO , as they represent the main combustible entities in the anode off-gas. The peak combustion temperature, laminar flame speed, and ignition delay times were calculated over a wide range of ϕ and water vapor percentages. The ϕ ranged from 0.6 to stoichiometric, in increments of 0.1, and the water vapor percentages ranged from 0% to 50%, in increments of 10%, to represent the actual composition of the SOFC anode off-gas. The initial temperature and pressure were fixed at 850 K and 14 bar and were taken from the experimental data representing the thermodynamic state at the end of the compression stroke of the CFR engine with a CR of 11. The peak combustion temperature as a function of ϕ and water vapor percentage is shown in Figure 11. The peak combustion temperature decreases as the water vapor percentage is increased at selected ϕ . Additionally, decreasing ϕ at

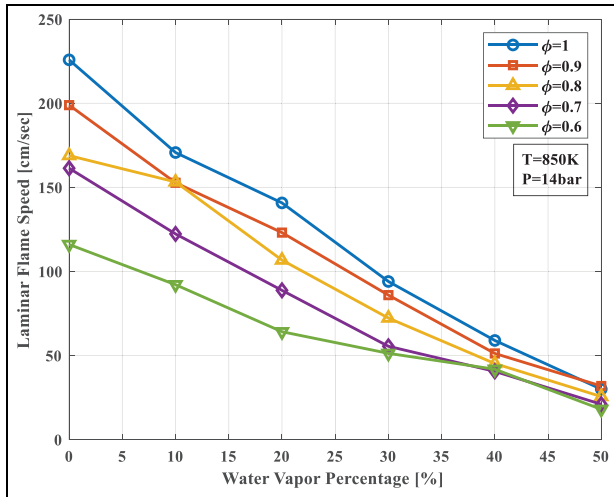


Figure 12. Laminar flame speed as a function of ϕ and water vapor percentage.

the same levels of water vapor percentage also resulted in lower peak combustion temperatures. Results from the modeling study exhibit similar trends as the results from the experimental data, as shown in Figure 9. Since the 0-D Chemkin model was developed based on a closed homogeneous and adiabatic constant volume combustion reactor, the peak combustion temperatures shown in Figure 11 are much higher than the temperatures that were calculated based on the experimental data.

Figure 12 displays the calculated laminar flame speed with respect to ϕ and water vapor percentage. As expected, the increase in water vapor percentage is shown to have a negative effect on laminar flame speed. The existence of higher water-vapor diluent in the anode off-gas composition reduces the energy density of the off-gas due to the reduction of the combustible components of H_2 and CO . Therefore, the laminar flame speed is largely reduced for higher water vapor percentages. Similarly, decreases in ϕ from stoichiometry also resulted in slower laminar flame speeds, which is attributed to the lower energy density of the fuel-air mixture, as a result of an increase in the airflow rate. The reduction in laminar flame speed resulted in slower flame propagating and combustion rates, and consequently, lower peak cylinder pressure and heat release rate, as shown in Figure 10.

The autoignition delay time, shown in Figure 13, is defined as the time in which a premixed homogeneous air-fuel mixture must be maintained at a certain pressure and temperature before the mixture autoignites. Investigation on the insight of autoignition delay time helps to gain a better understanding of the effects of fuel properties on the ignition and combustion characteristics, especially in SI engines. As shown in Figure 13, an initial decrease in ignition delay time is observed with up to 30% of water vapor addition for the mixture. Addition of water vapor beyond 30% results in an increase in ignition delay time. The initial decrease

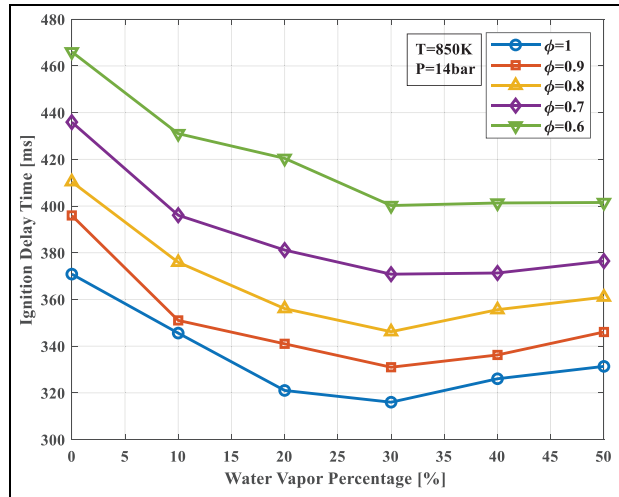


Figure 13. Ignition delay time as a function of ϕ and water vapor percentage.

in the ignition delay time with water vapor addition up to 30% can be attributed to the dissociation of H_2O at elevated temperatures and pressures, thus producing H , O , and OH radicals; the latter promote chemical reaction rates, consequently decreasing ignition delay. Beyond this initial decrease in ignition delay, the thermal effects of adding water vapor dominates the chemical reaction process, and the ignition delay time starts to increase again due to the significantly lowered flame temperature.

Conclusions

In this experimental study, a spark-ignited CFR engine was used to investigate combustion with simulated anode off-gas from a representative SOFC stack, at three different compression ratios. The effect of anode off-gas compositions, water vapor contents, and compression ratios on engine performance, pollutant emissions, and efficiencies was quantified and analyzed. The following can be summarized as important scientific discoveries and conclusions:

- The experimental results presented in this study reveal that the conventional SI engine can be used downstream of a SOFC stack to generate additional power, thus confirming the feasibility of a SOFC-ICE hybrid power plant to improve the combined electrical efficiency.
- A SOFC, simulated dry surrogate, anode off-gas was successfully used as a fuel in a spark-ignition engine. Results show stable combustion can be achieved and yield a net indicated fuel conversion efficiency of 31.3% at a CR of 13:1, with minimal NO_x emissions, zero hydrocarbon, and soot emissions.
- While anode off-gas is a diluted fuel mixture that reduces the volumetric efficiency of a SI engine, its

combustion results in low emissions formation, equal to or lower than low-temperature combustion concepts.

- Both experimental data and Chemkin simulation results revealed that the presence of up to 30% water vapors in the fuel content actually helps to shorten the ignition delay period, and consequently the combustion duration. However, the presence of water vapors higher than 30% will negatively affect the combustion duration, efficiencies, as well as exhaust emissions.
- The use of a conventional SI mode provides a simpler, more robust, and direct control mechanism over the start of combustion and heat release rate. Hence, SI allows for a wider operating range than the chemical reaction control mechanism of the HCCI mode; this decreases the complexity of controlling a hybrid power generation plant, especially during transient operating conditions.
- The CFR engine used for the experimental study is representative of an older SI engine design with only two valves, a side-mounted spark plug, and a quiescent combustion chamber. It is expected that the efficiency of an anode off-gas can be further improved by selecting a modern engine with increased turbulent motion, modern valvetrain, improved combustion chamber design, and a centrally mounted spark plug.

Acknowledgements

The authors would like to thank Dr. Sotirios Mamalis, previously at Stony Brook University for the representative hybrid SOFC system design, as well as Dr. Scott Swartz and Mr. Gene Arkenberg from Nexceris for providing details regarding the composition and operating conditions of the anode off-gas from a representative SOFC stack used for power generation. Additionally, the authors thank Dr. Benjamin John Lawler and Mr. Brain Gainey of Clemson University for sharing their knowledge in system-level modeling of hybrid SOFC-ICE.



Declaration of conflicting interests

The author(s) declared no potential conflicts of interest with respect to the research, authorship, and/or publication of this article.

Funding

The author(s) disclosed receipt of the following financial support for the research, authorship, and/or publication of this article: The experimental and numerical studies were conducted at Stony Brook University and funded by the United States Department of Energy (ARPA-E INTEGRATE) project, award number of (DE-AR0000959).

ORCID iDs

Zhongnan Ran  <https://orcid.org/0000-0001-5813-3293>
Dimitris Assanis  <https://orcid.org/0000-0001-5506-806X>

References

1. Longwell JP, Rubin ES and Wilson J. Coal: energy for the future. *Prog Energy Combust Sci* 1995; 21: 269–360.
2. Bizon N and Thounthong P. Fuel economy using the global optimization of the fuel cell hybrid power systems. *Energy Convers Manag* 2018; 173: 665–678.
3. Sulaiman N, Hannan M, Mohamed A, Ker PJ, Majlan E and Daud WW. Optimization of energy management system for fuel-cell hybrid electric vehicles: issues and recommendations. *Appl Energy* 2018; 228: 2061–2079.
4. Song K, Chen H, Wen P, Zhang T, Zhang B and Zhang T. A comprehensive evaluation framework to evaluate energy management strategies of fuel cell electric vehicles. *Electrochim Acta* 2018; 292: 960–973.
5. Lee YD, Ahn KY, Morosuk T and Tsatsaronis G. Environmental impact assessment of a solid-oxide fuel-cell-based combined-heat-and-power-generation system. *Energy* 2015; 79: 455–466.
6. Brouwer J. *Hybrid gas turbine fuel cell systems*. Chapter 4. The Gas Turbine Handbook, National Fuel Cell Research Center, Irvine, CA: University of California, 2003.
7. Gainey B and Lawler B. A fuel cell free piston gas turbine hybrid architecture for high-efficiency, load-flexible power generation. *Appl Energy* 2021; 283: 116242.
8. Cheddie DF. Thermo-economic optimization of an indirectly coupled solid oxide fuel cell/gas turbine hybrid power plant. *Int J Hydrog Energy* 2011; 36: 1702–1709.
9. Inui Y, Matsumae T, Koga H and Nishiura K. High performance SOFC/GT combined power generation system with CO₂ recovery by oxygen combustion method. *Energy Convers Manag* 2005; 46: 1837–1847.
10. Harvey S. P. and Richter H. J. Gas turbine cycles with solid oxide fuel cells—part II: a detailed study of a gas turbine cycle with an integrated internal reforming solid oxide fuel cell. *ASME. J Energy Resour Technol* 1994; 116(4): 312–318.
11. Chan S, Ho H and Tian Y. Multi-level modeling of SOFC–gas turbine hybrid system. *Int J Hydrog Energy* 2003; 28: 889–900.
12. Kuchonthara P, Bhattacharya S and Tsutsumi A. Combinations of solid oxide fuel cell and several enhanced gas turbine cycles. *J Power Sources* 2003; 124: 65–75.
13. Calise F, Palombo A and Vanoli L. Design and partial load exergy analysis of hybrid SOFC–GT power plant. *J Power Sources* 2006; 158: 225–244.
14. Reitz R, Ogawa H, Payri R, et al. *IJER editorial: the future of the internal combustion engine*. London, England: SAGE Publications, 2020.
15. Vora SD. Office of fossil energy's solid oxide fuel cell program overview. In: *15th annual SECA workshop*. Pittsburgh, PA: National Energy Technology Laboratory, 2014, pp.22–23.
16. Lee YD, Ahn KY, Morosuk T and Tsatsaronis G. Exergetic and exergoeconomic evaluation of an SOFC-engine hybrid power generation system. *Energy* 2018; 145: 810–822.
17. Fyffe JR, Donohue MA, Regalbuto MC and Edwards CF. Mixed combustion–electrochemical energy conversion for high-efficiency, transportation-scale engines. *Int J Engine Res* 2017; 18: 701–716.
18. Rodríguez, JC, Harun, NF, Zhou, N, Sabolsky, E, & Tucker, D. System Analysis of a 100kW Internal Combustion Engine (ICE) Solid Oxide Fuel Cell (SOFC)

- Hybrid Configuration. In: *Proceedings of the ASME 2020 Power Conference collocated with the 2020 International Conference on Nuclear Engineering*. ASME 2020 Power Conference. Virtual, Online. August 4–5, 2020. V001T12A004. ASME.
19. Choi W, Kim J, Kim Y, Kim S, Oh S and Song HH. Experimental study of homogeneous charge compression ignition engine operation fuelled by emulated solid oxide fuel cell anode off-gas. *Appl Energy* 2018; 229: 42–62.
 20. Zhu P, Yao J, Qian C, et al. High-efficiency conversion of natural gas fuel to power by an integrated system of SOFC, HCCI engine, and waste heat recovery: thermodynamic and thermo-economic analyses. *Fuel* 2020; 275: 117883.
 21. Park SH, Lee YD and Ahn KY. Performance analysis of an SOFC/HCCI engine hybrid system: system simulation and thermo-economic comparison. *Int J Hydrog Energy* 2014; 39: 1799–1810.
 22. Zhao F, Asmus TN, Assanis DN, Dec JE, Eng JA and Najt PM. Homogeneous charge compression ignition (HCCI) engines. SAE technical paper 2003-03-03, 2003.
 23. Toulson E, Schock HJ and Attard WP. A review of pre-chamber initiated jet ignition combustion systems. SAE technical paper 2010-01-2263, 2010.
 24. Assanis D, Engineer N, Neuman P and Wooldridge M. Computational development of a dual pre-chamber engine concept for lean burn combustion. SAE technical paper 2016-01-2242, 2016.
 25. Chuahy FD and Kokjohn SL. Solid oxide fuel cell and advanced combustion engine combined cycle: a pathway to 70% electrical efficiency. *Appl Energy* 2019; 235: 391–408.
 26. Kim J, Kim Y, Choi W, Ahn KY and Song HH. Analysis on the operating performance of 5-kW class solid oxide fuel cell-internal combustion engine hybrid system using spark-assisted ignition. *Appl Energy* 2020; 260: 114231.
 27. Ran Z, Assanis D, Hariharan D and Mamalis S. Experimental study of spark-ignition combustion using the anode off-gas from a solid oxide fuel cell. SAE technical paper 2020-01-0351, 2020.
 28. Ran Z, Hariharan D, Lawler B and Mamalis S. Experimental study of lean spark ignition combustion using gasoline, ethanol, natural gas, and syngas. *Fuel* 2019; 235: 530–537.
 29. Heywood JB. *Internal combustion engine fundamentals*. 2nd ed. New York: McGraw-Hill Education, 2018.
 30. Haase H. *Electrostatic hazards: their evaluation and control*. Wiley-VCH, 1977.
 31. Babrauskas V and Handbook I. *Society of fire protection engineers*. Fire Science Publishers, 2003.
 32. Kéromnès A, Metcalfe WK, Heufer KA, et al. An experimental and detailed chemical kinetic modeling study of hydrogen and syngas mixture oxidation at elevated pressures. *Combust Flame* 2013; 160: 995–1011.